Article

A Highly Stable-Output Kilohertz Femtosecond Hard X-ray Pulse Source for Ultrafast X-ray Diffraction

Di Zhao [1,†], Pengxian You [1,2,†], Jing Yang [1,*], Junhong Yu [1], Hang Zhang [1], Min Liao [2] and Jianbo Hu [1,*]

[1] Laboratory for Shock Wave and Detonation Physics, Institute of Fluid Physics, China Academy of Engineering Physics, Mianyang 621900, China; zhaodi19@gscaep.ac.cn (D.Z.); 201931000127@smail.xtu.edu.cn (P.Y.); jyu012@e.ntu.edu.sg (J.Y.); zhanghang@caep.cn (H.Z.);

[2] School of Materials Science and Engineering, Xiangtan University, Xiangtan 411105, China; mliao@xidian.edu.cn

[*] Correspondence: yangjing0102@caep.cn (J.Y.); jianbo.hu@caep.cn (J.H.)

[†] These authors contributed equally to this work

Abstract: Femtosecond hard X-ray pulses generated by laser-driven plasma sources are eminently suitable to probe structural dynamics due to the angstrom spatial resolution and sub-picosecond time resolution. However, the insufficient flux of X-ray photons and high pulse-to-pulse instability compared with the large-scale ultrashort X-ray source, such as X-ray free-electron laser and synchrotrons, largely restricts its applications. In this work, we have optimized automation control and mechanical designs to significantly enhance the reliability and photon flux in our femtosecond laser plasma-induced X-ray source. Specifically, the optimized source provides a reliable pulse-to-pulse stability with a fluctuation of less than 1% (root-mean-square) and a total flux of Cu-K_α X-ray photons above 10^{11} photons/s. To confirm its functionality, ultrafast X-ray diffraction experiments are conducted on two different samples and the high consistency with previous results verifies the system's superior performance.

Keywords: laser–plasma interaction; ultrashort laser pulse; ultrafast X-ray diffraction; pulse-to-pulse stability

1. Introduction

Ultrafast X-ray diffraction (UXRD), which combines the sub-picosecond temporal resolution and sub-angstrom spatial resolution, can be used as a camera to real-time map atomic motions in reciprocal space and thus decipher those nonequilibrium phenomena in condensed matter physics, such as photoinduced phase transitions [1,2] and photoacoustic stress propagation [3–5]. Large-scale accelerator-generated X-ray sources (e.g., synchrotrons or X-ray free-electron laser (XFEL)) with high brightness and good stability are ideal for time-resolved diffraction [6–8], but their high cost and limited beamtime limit the extensive use. Laser plasma-based X-ray sources with advantages of ultrashort pulse duration and low cost then emerge as a valuable supplement to large-scale accelerator-based sources. However, the relatively low brightness and flux stability of ultrashort X-ray pulses greatly hinder its performance in measuring poor quality single-crystal or polycrystalline samples considering that UXRD usually needs a long time to acquire enough diffracted X-ray photons for a high-quality diffraction pattern. In fact, the flux of laser plasma X-ray sources is generally on the order of 10^{10} photons/s [9–11].

Since the 21 century, the development of femtosecond laser technology has enabled the generation of ultrashort hard X-ray pulses with a kilohertz repetition rate [12–16]. Since then, substantial efforts have been devoted to improving the reliability and photon flux in the femtosecond laser plasma-induced X-ray source, mainly including (i) optical designs to change the wavelength of laser pulses from 800 nm to mid-infrared [17,18] or

increase the contrast between the pre-pulse and the main pulse [19,20]; and (ii) mechanical designs to enhance the laser pointing stability on the target foil surface [12]. Nevertheless, the fluctuation of pulse-to-pulse stability of photon flux in hard X-ray sources is still larger than 2% (root-mean-square (RMS)) and the total photon flux of less than 10^{11} photons/s is serval orders of magnitude lower than one in large-scale ultrashort X-ray sources [10,12,16,21]. These key metrics largely restrict the application of laser-plasma-based hard X-ray pulse sources and further improvements are required. In this work, we have designed and demonstrated a novel, highly compact Cu-K$_\alpha$ X-ray ultrashort source operating at a kHz repetition rate, which provides a reliable pulse-to-pulse stability with a fluctuation of 1% (RMS) and a total flux of Cu-K$_\alpha$ X-ray photons above 10^{11} photons/s. The superior performance of our novel hard X-ray pulses is mainly due to the optimization of both the software and hardware. From a hardware perspective, an independent copper reaction chamber is designed to prevent the spread of debris. Furthermore, a homemade target tape driving system based on a stepping motor and the laser displacement sensor is introduced to ensure the smooth moving of the target tape. While from a software perspective, the home-built software that can simultaneously control the target tape driver, monitor laser focal spot/optical alignment, and automatically obtain transient data traces, is adopted to ensure the stable and efficient operation of our X-ray sources. To verify the functionality of our X-ray pulse sources, UXRD experiments on different samples are conducted, which show a good consistency with previous results obtained in other X-ray sources.

2. Results and Discussion

2.1. Optimization of the Laser-Plasma-Based Hard X-ray Pulse Source

As shown in Figure 1a,b, the prototype table-top plasma X-ray source consists of a U-shaped steel vacuum chamber operating at a pressure of 10^{-4} mbar (the size is 67 cm × 55 cm × 15 cm) and a commercial 1 kHz Ti: sapphire femtosecond laser system which provides *p*-polarized 35 fs laser pulses with a center wavelength of 800 nm and a maximum pulse energy output up to 13 mJ. The output beam from the laser system is divided into two pulses by the beam splitter with an intensity ratio of 1:9. The weak pulse at 800 nm (the wavelength can be tuned from the ultraviolet to the mid-infrared by nonlinear frequency conversion based on experimental requirements) is utilized as the pump beam to initiate the dynamics in the sample under concern, while the strong one is focused on the 20 μm-thickness Cu foil target (moving at a speed of 40 mm/s) by an off-axis parabolic mirror (OAP, which is out of the chamber with an effective focal length of 101.2 mm) to generate X-ray pulses. The laser focal spot is measured by the beam profiler (see Figure 1c), indicating that the vertical and horizontal Full-Width Half-Maximum (FWHM) is 7.8 μm and 8.1 μm, respectively. As shown in Figure 1d, the spectrum of the generated X-ray pulse is measured with a silicon-based pin photon detector with a 300 μm diameter lead aperture and a 400 μm thick aluminum foil is placed in front of the detector to ensure that the data acquisition is under the single-photon counting mode. As expected, the spectrum with a high signal-to-noise ratio is obtained, which is dominated by Cu characteristic radiations (K$_\alpha$ and K$_\beta$) superimposed on a small bremsstrahlung background. To monochromize the X-ray pulse, one can use a nickel foil (8 μm) to filter the Cu-K$_\beta$ line with a 40% loss in intensity (the red curve in Figure 1d).
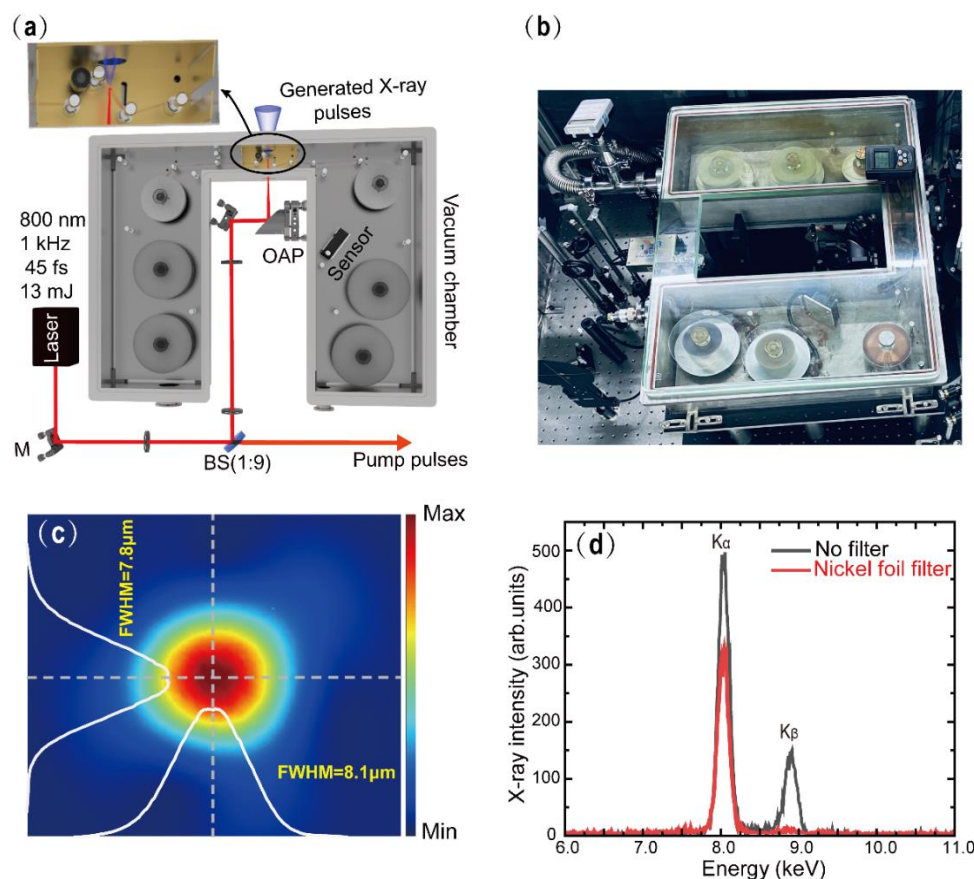
Figure 1. (**a**) Schematic diagram of the table-top laser-plasma-based X-ray source. (**b**) Top view of the X-ray generation vacuum chamber. (**c**) Image of the laser focal spot. The white lines show that the Full-With Half-Maximum (FWHM) values in the vertical and horizontal are 7.8 and 8.1 μm, respectively. (**d**) The X-ray pulse spectrum. The black and red lines represent the spectrum without and with an 8 μm nickel foil filter.

As mentioned above, a key issue in hard X-ray sources is flux instability. Although sources with a solid target tape are relatively simple to operate in comparison with the liquid target, they generate metallic debris. A continuously moving plastic tape is thus required to take away the generated debris to maintain the optical transmittance of the chamber entrance. On the other hand, it is well known that the moving speed of the copper tape also affects the conversion efficiency from laser to X-ray [12]. Therefore, it is critical to maintain the copper tape at a constant moving speed. To reach this aim, we have introduced several rotatable deflection rolls to hold the target tape as stable as possible, which combines static and rolling friction to keep the tightness of the target tape to avoid any sudden change in the rotating speed. Additionally, then, similar to the cassette player, a pinch roller in the reaction chamber is used to maintain the surface stability of the copper tape. Moreover, we redesigned the driving system to include a high-precision laser displacement sensor with an accuracy of 2.5 μm and a sampling period of 200 μs. This sensor is installed inside the vacuum chamber to measure the radius of the active copper tape reel during the moving process. Based on the conversion relation between the line speed and the angular velocity, we obtain the real-time radius value change and then determine the number of rotation pulses at a unit time of the stepping motor using home-built software. In such a way, we can actively control the moving speed of the copper tape.

Besides the mechanical factors, the fluctuation of the laser pulse itself cannot be ignored. To reduce the laser pointing drift on the copper tape due to the temperature or other environmental changes, we use two pairs of diaphragms placed in the optical path to confine the laser beam direction actively. Benefitting from these optimizations, we have

successfully obtained a relatively stable X-ray flux in a long term. As shown in Figure 2a, the maximum fluctuation of generated Cu-K$_\alpha$ X-ray flux in 100 min is less than 10 percent, which is equivalent to 1% (RMS). It is worth mentioning that these designs also ensure a high total flux of Cu-K$_\alpha$ X-ray photons above 10^{11} photons/s by optimizing the laser focal size and the moving speed of the copper tape. By assuming an isotropic production of Cu-K$_\alpha$ radiation at a solid angle of 4π, we estimate the laser intensity-dependent flux of Cu-K$_\alpha$ photons (see Figure 2b). The nearly proportional relationship between laser intensity and X-ray photon flux suggests that vacuum heating is dominant in the range of intensities accessible in our experiments [22].
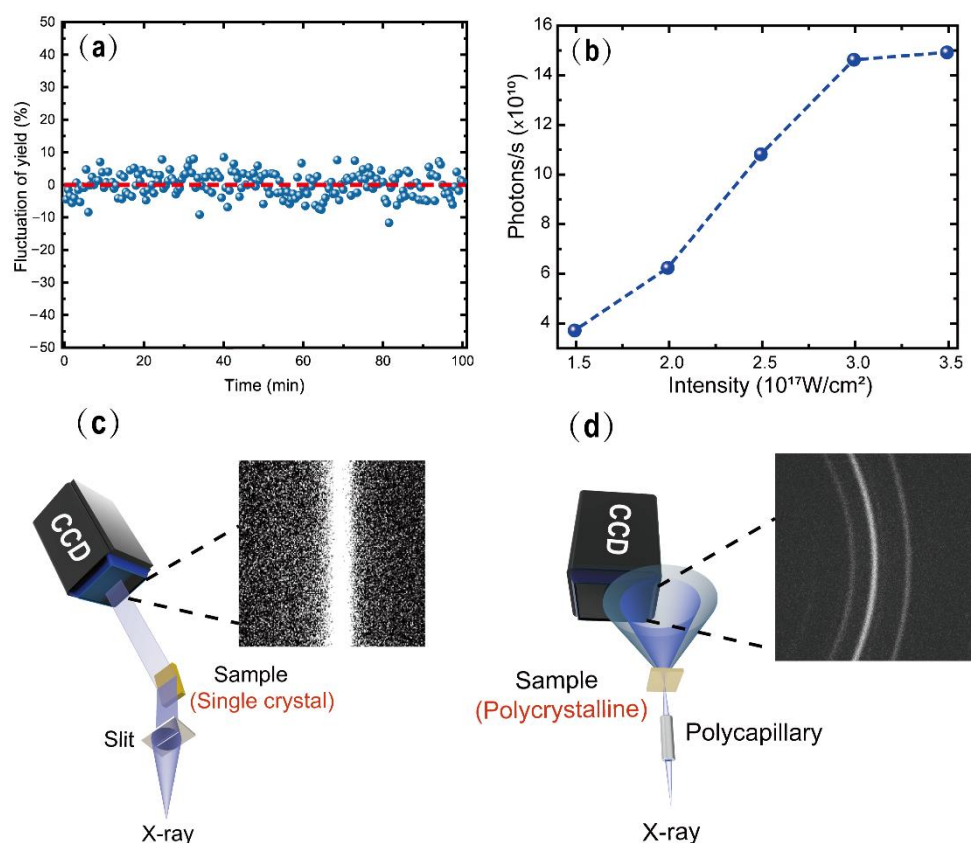

Figure 2. (**a**) The fluctuation of generated Cu-K$_\alpha$ X-ray flux within 100 min (blue dot) corresponding to the average output (red line). (**b**) The laser pump intensity dependence of the generated X-ray photon flux. (**c**) The reflection geometry of X-ray diffraction, in which the generated X-ray is passing through a tantalum slit and diffracted off a single-crystal Au film. The integration time of the measured diffraction pattern is 20 s. (**d**) The transmission geometry of X-ray diffraction, in which the generated X-ray is collected by a polycapillary X-ray optics and then diffracted off a polycrystalline Cu tape. The integration time of the measured diffraction pattern is 300 s.

To test the generated X-ray pulses, we have performed the static X-ray diffraction (XRD) experiments on both single-crystal Au and polycrystalline Cu samples. As shown in Figure 2c, XRD of a single crystal is taken with a reflection geometry. In this geometry, we shaped the emitted Cu-K$_\alpha$ radiation by a 300 μm wide tantalum slit mounted 35 mm away from the X-ray source and then diffracted off the Au (111) film mounted 156 mm away from the slit. The X-ray diffraction signal is captured by the X-ray CCD camera with 2048 × 2048 pixels (with a pixel size of 13.5 μm) located 191 mm away from the sample. With the exposure time of 20 s, an ideal signal-to-noise Bragg diffraction pattern has been obtained, as shown in Figure 2c. While for polycrystalline sample, a transmission geometry is taken, as shown in Figure 2d. A polycapillary X-ray optics was used to focus Cu-K$_\alpha$

radiation on a 20 μm polycrystalline Cu foil with a 600 μm spot in diameter. Thanks to the polycapillary X-ray optics with the magnification of 300 gain, about 10^7 X-ray photons/s on the sample are available. In this geometry, the X-ray CCD camera is mounted about 10 mm behind the sample, and the diffraction pattern shown in Figure 2d was acquired with the exposure time of 300 s. These results indicate the feasibility of the generated X-ray pulses to perform UXRD measurements on different types of samples ranging from single crystal to polycrystalline.

2.2. Ultrafast X-ray Diffraction Measurements

In the following, we demonstrate UXRD experiments conducted on two different samples using our optimized femtosecond X-ray source.

We first study a 200 nm thick Au (111) single crystal film grown on the mica substrate. The dynamics are triggered by a 400 nm pump pulse with an energy of 200 μJ. The corresponding penetration depth is 17 nm [10,23] and the diameter of the optical pump spot on the sample is 2 mm, which is much larger than the width of the X-ray strip on the sample to ensure the homogenous excitation in the probed regime. To achieve a good signal-to-noise ratio, each Bragg diffraction image at different delay times is obtained by two-cycle accumulations. The exposure time of each image of one cycle is 20 s. The diffraction patterns include irradiated area and non-irradiated area of the film, and the latter is used as the reference for normalization.

The electron–lattice interaction in Au-film after femtosecond optical excitation has been widely studied in detail [10,24–27]. When the optical pulse irradiates into the surface layer of the film, the deposited laser energy is first absorbed by the surface electrons, leading to the heating of electrons to a very high temperature in an ultrashort period, and then heating the lattice by the electron–lattice interaction. On the other hand, the optical excitation induces a large transient elastic force at the surface [24], which only lasts during the early electron nonequilibrium (1 ps to 2 ps), and the blast wave generated by this elastic force will propagate into the depth with the sound velocity, inducing strain wave along its path.

The measured transient θ–2θ scan curves for the delay time ranging from −140 ps to 390 ps are presented in Figure 3a. The white dotted line indicates the change in the center of the Bragg peak, which is extracted based on the single Gaussian function fitting. The variation of inter-atomic spacing of a 200-nm Au (111) crystal as a function of the pump-probe time delay is shown in Figure 3b. A shift of the diffraction angles and a slight broadening are observed when $t > 0$ ps. A shift towards a smaller diffraction angle indicates lattice expansion, and the maximum shift is reached at 60 ps after excitation [10]. Following the maximum lattice expansion, we have fitted the experimental data using the sine-damping function:

$$y = y_0 + Ae^{-\frac{x}{t_0}}\sin(\pi - \frac{x - x_x}{w})$$

where y_0 is the fitting constant (7.9×10^{-4}), w is the oscillation period (59.5 ps), t_0 is the decay lifetime (120.5 ps), and A is the oscillation amplitude (7.8×10^{-4}). The fitting result with an R-square of −0.96 indicates that damped oscillations appear with a period of 121 ps, implying lattice breathing along the surface normal [9,24]. The measured characteristic time (121 ps) is in good agreement with the theoretical calculation: $\tau_{ac} = 2d/c_s = 123$ ps, where $d = 200$ nm is the sample thickness and $c_s = 3.24$ km/s is the longitudinal velocity of the acoustic wave in gold. Such oscillations stem from the blast waves traveling back and forth through the film along the (111) direction and the damping in oscillations amplitude is due to the finite acoustic transmission into the substrate.
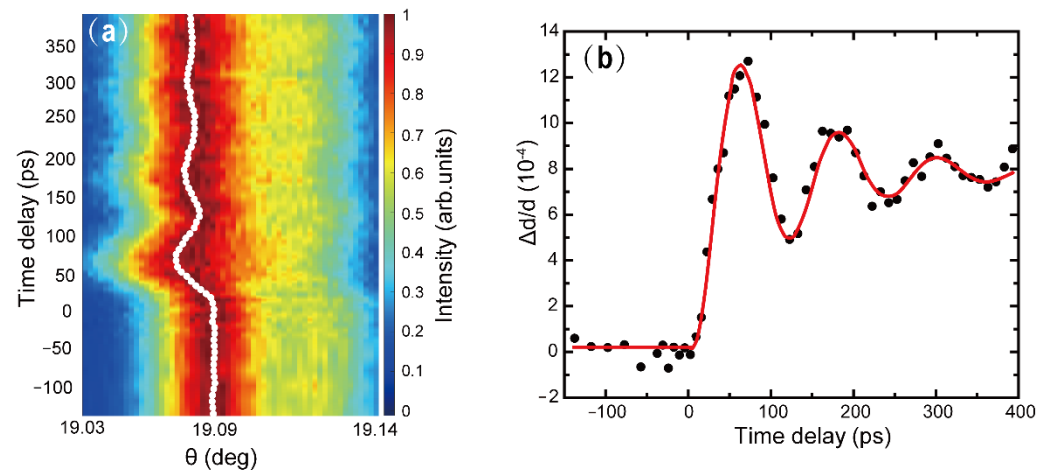
Figure 3. (**a**) Transient θ-2θ scans for different delay times of −140 ps < t < 390 ps. The white dotted line indicates the center of the Bragg peaks. (**b**) Variation of inter-atomic spacing of a 200-nm Au (111) crystal as a function of pump-probe time delay. The fitting by a sine-damping function is shown as a solid red line.

In the second pump-probe experiment, the sample is composed of a 105 nm thick (110) SrRuO$_3$ (SRO) film epitaxially grown on a (110) SrTiO$_3$ (STO) substrate. We excited the SRO layer with 800 nm femtosecond laser pulses. The penetration depth is about 52 nm [28]. The focal spot diameter is 2 mm on the sample with an excitation fluence of 13 mJ/cm². Unlike Au film, imperfect crystal growth and a smaller cross-section in X-ray diffraction lead to the broadening of diffraction peaks and a decrease in diffraction efficiency during our data collection process. As a result, a total of fifteen-cycle acquisitions are required to achieve a good signal-to-noise ratio in this experiment. The acquisition time of an image in each cycle is 30 s.

The photoinduced dynamics are represented by the transient θ–2θ scans shown in Figure 4a. The Bragg peak becomes much broader/weaker and moves to a lower angle following the optical excitation [29]. The absorption of the pump pulse leads to a quasi-instantaneous temperature jump, resulting in inhomogeneous heating of the film and strains, which modify the interplanar spacing. Such transient changes in lattice geometry give rise to changes in the X-ray diffraction pattern. As shown in Figure 4b, the observed maximum change in the intensity corresponds to the maximum peak shift to a smaller angle, indicating the maximum lattice expansion of $\Delta d/d \approx 0.4\%$. The characteristic timescale is determined by $\tau_{ac} = d/v_s = 16.7$ ps, where d is the layer thickness (105 nm) and vs. = 6.3 km/s is the longitudinal sound velocity [4,28,30]. Thereafter, the peak intensity is followed by a slight backshift and then reaches a new equilibrium position, which indicates a monotonical decrease of strain until the equilibrium state is reached. This process is determined by the pure thermal expansion and will continue until it relaxes to ambient temperature via heat diffusion into the substrate on a nanosecond or even microsecond timescale [31,32].
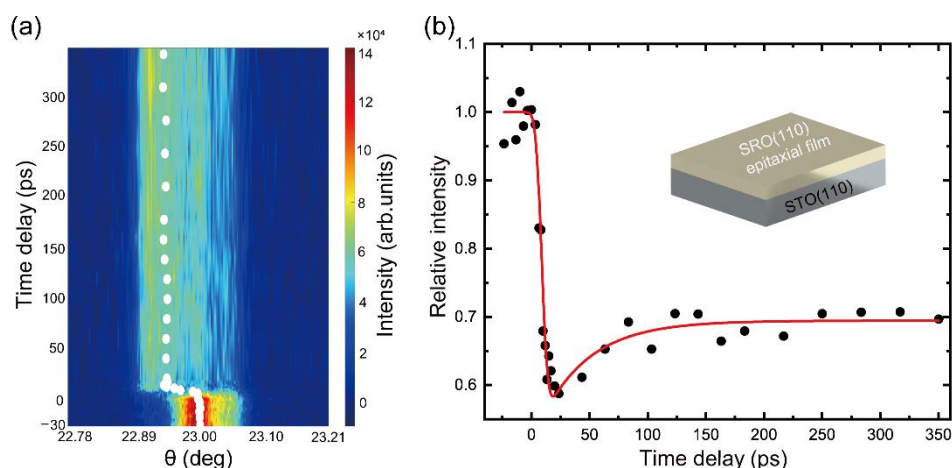
Figure 4. (**a**) Transient θ–2θ scans for different delay times of −30 ps < *t* < 350 ps. The white dotted line indicates the center of the Bragg peaks. (**b**) Normalized relative Bragg peak intensity variation of a 105-nm SRO (110) film with different pump-probe time delays, the solid red line represents an exponential data fitting.

3. Conclusions

This paper described an optimized femtosecond hard X-ray plasma source working at a kilohertz repetition rate, which is driven by a commercial Ti: sapphire laser system. Through the optimized designs of an independent copper reaction chamber, a home-made target tape driving system, and the home-built system control/monitor software, a highly compact Cu-K$_\alpha$ X-ray source has been demonstrated, which can provide a reliable pulse-to-pulse stability with a fluctuation of 1% (RMS) and a total flux of Cu-K$_\alpha$ X-ray photons above 10^{11} photons/s. To test the functionality of our X-ray sources, static and time-resolved X-ray diffraction experiments on both single crystal and polycrystalline samples are performed, which yield good consistency with previous results obtained in other ultrashort X-ray sources.

References

1. Zhang, H.; Zhang, Y.; Li, R.; Yu, J.; Dong, W.; Chen, C.; Wang, K.; Tang, X.; Chen, J. Room temperature hidden state in a manganite observed by time-resolved X-ray diffraction. *Npj Quantum Mater.* **2019**, *4*, 31.
2. Rousse, A.; Rischel, C.; Fourmaux, S.; Uschmann, I.; Sebban, S.; Grillon, G.; Balcou, P.; Förster, E.; Geindre, J.P.; Audebert, P.; et al. Non-thermal melting in semiconductors measured at femtosecond resolution. *Nature* **2001**, *410*, 65–68.
3. Sokolowski-Tinten, K.; Blome, C.; Dietrich, C.; Tarasevitch, A.; von Hoegen, M.H.; von der Linde, D.; Cavalleri, A.; Squier, J.; Kammler, M. Femtosecond X-ray measurement of ultrafast melting and large acoustic transients. *Phys. Rev. Lett.* **2001**, *87*, 225701.
4. Schick, D.; Bojahr, A.; Herzog, M.; Gaal, P.; Vrejoiu, I.; Bargheer, M. Following strain-induced mosaicity changes of ferroelectric thin films by ultrafast reciprocal space mapping. *Phys. Rev. Lett.* **2013**, *110*, 095502.
5. Schick, D.; Herzog, M.; Wen, H.; Chen, P.; Adamo, C.; Gaal, P.; Schlom, D.G.; Evans, P.G.; Li, Y.; Bargheer, M. Localized excited charge carriers generate ultrafast inhomogeneous strain in the multiferroic BiFeO$_3$. *Phys. Rev. Lett.* **2014**, *112*, 097602.
6. Schoenleins, R.W.; Chattopadhyay, S.; Chong, H.H.W.; Glover, T.E.; Heimann, P.A.; Shank, C.V.; Zholents, A.A.; Zolotorev, M.S. Generation of femtosecond pulses of synchrotron radiation. *Science* **2000**, *287*, 2237–2240.

7. Ishikawa, T.; Aoyagi, H.; Asaka, T.; Asano, Y.; Azumi, N.; Bizen, T.; Kumagai, N. A compact X-ray free-electron laser emitting in the sub-ångström region. *Nat. Photonics* **2012**, *6*, 540–544.

8. Marangos, J.P. Introduction to the new science with X-ray free electron lasers. *Contemp. Phys.* **2011**, *52*, 551–569.

9. Lu, W.; Nicoul, M.; Shymanovich, U.; Brinks, F.; Afshari, M.; Tarasevitch, A.; von der Linde, D.; Sokolowski-Tinten, K. Acoustic response of a laser-excited polycrystalline Au-film studied by ultrafast Debye–Scherrer diffraction at a table-top short-pulse x-ray source. *AIP Adv.* **2020**, *10*, 035015.

10. Guo, X.; Jiang, Z.; Chen, L.; Chen, M.L.; Xin, J.; Rentzepis, P.M.; Chen, J. Ultrafast structural dynamics studied by kilohertz time-resolved x-ray diffraction. *Chin. Phys. B* **2015**, *24*, 108701.

11. Bargheer, M.; Zhavoronkov, N.; Woerner, M.; Elsaesser, T. Recent progress in ultrafast X-ray diffraction. *Chemphyschem A Eur. J. Chem. Phys. Phys. Chem.* **2006**, *7*, 783–792.

12. Zamponi, F.; Ansari, Z.; Schmising, C.V.K.; Rothhardt, P.; Zhavoronkov, N.; Woerner, M.; Elsaesser, T.; Bargheer, M.; Trobitzsch-Ryll, T.; Haschke, M. Femtosecond hard X-ray plasma sources with a kilohertz repetition rate. *Appl. Phys. A* **2009**, *96*, 51–58.

13. Silies, M.; Witte, H.; Linden, S.; Kutzner, J.; Uschmann, I.; Förster, E.; Zacharias, H. Table-top kHz hard X-ray source with ultra-short pulse duration for time-resolved X-ray diffraction. *Appl. Phys. A* **2009**, *96*, 59–67.

14. Hagedorn, M.; Kutzner, J.; Tsilimis, G.; Zacharias, H. High-repetition-rate hard X-ray generation with sub-millijoule femtosecond laser pulses. *Appl. Phys. B* **2003**, *77*, 49–57.

15. Korn, G.; Thoss, A.; Stiel, H.; Vogt, U.; Richardson, M. Ultrashort 1-kHz laser plasma hard x-ray source. *Opt. Lett.* **2002**, *27*, 866–868.

16. Zhavoronkov, N.; Gritsai, Y.; Korn, G.; Elsaesser, T. Ultra-short efficient laser-driven hard X-ray source operated at a kHz repetition rate. *Appl. Phys. B* **2004**, *79*, 663–667.

17. Koç, A.; Hauf, C.; Woerner, M.; Grafenstein, L.; Ueberschaer, D.; Bock, M.; Griebner, U.; Elsaesser, T. Compact high-flux hard X-ray source driven by femtosecond mid-infrared pulses at a 1 kHz repetition rate. *Opt. Lett.* **2021**, *46*, 210–213.

18. Weisshaupt, J.; Juvé, V.; Holtz, M.; Ku, S.; Woerner, M.; Elsaesser, T.; Ališauskas, S.; Pugžlys, A.; Baltuška, A. High-brightness table-top hard X-ray source driven by sub-100-femtosecond mid-infrared pulses. *Nat. Photonics* **2014**, *8*, 927–930.

19. Chen, L.M.; Kando, M.; Xu, M.H.; Li, Y.T.; Koga, J.; Chen, M.; Xu, H.; Yuan, X.H.; Dong, Q.L.; Sheng, Z.M.; et al. Study of X-ray emission enhancement via a high-contrast femtosecond laser interacting with a solid foil. *Phys. Rev. Lett.* **2008**, *100*, 045004.

20. Gibbon, P.; Bell, A.R. Collisionless absorption in sharp-edged plasmas. *Phys. Rev. Lett.* **1992**, *68*, 1535.

21. Zhu, C.; Tan, J.; He, Y.; Wang, J.; Li, Y.; Lu, X.; Li, Y.; Chen, J.; Chen, M.L.; Zhang, J. Ultrafast structural dynamics using time-resolved x-ray diffraction driven by relativistic laser pulses. *Chin. Phys. B* **2021**, *30*, 098701.

22. Chen, L.M.; Zhang, J.; Dong, Q.L.; Teng, H.; Liang, T.J.; Zhao, L.Z.; Wei, Z.Y. Hot electron generation via vacuum heating process in femtosecond laser–solid interactions. *Phys. Plasmas* **2001**, *8*, 2925–2929.

23. Chen, J.; Chen, W.K.; Tang, J. Time-resolved structural dynamics of thin metal films heated with femtosecond optical pulses. *Proc. Nat. Acad. Sci. USA* **2011**, *108*, 18887–18892.

24. Chen, J.; Chen, W.K.; Tang, J.; Rentzepis, P.M. Hot electrons blast wave generated by femtosecond laser pulses on thin Au(1 1 1) crystal, monitored by subpicosecond X-ray diffraction. *Chem. Phys. Lett.* **2006**, *419*, 374–378.

25. Hu, J.; Karam, T.E.; Blake, G.A.; Zewail, A.H. Ultrafast lattice dynamics of single crystal and polycrystalline gold nanofilms☆. *Chem. Phys. Lett.* **2017**, *683*, 258–261.

26. Gan, Y.; Che, J.K. Thermomechanical wave propagation in gold films induced by ultrashort laser pulses. *Mech. Mater.* **2010**, *42*, 491–501.

27. Hartland, G.V.; Hu, M.; Sader, J.E. Softening of the symmetric breathing mode in gold particles by laser-induced heating. *J. Phys. Chem. B* **2003**, *107*, 7472–7478.

28. Schick, D.; Bojahr, A.; Herzog, M.; Shayduk, R.; Schmising, C.V.K.O.; Bargheerac, M. Udkm1Dsim—A simulation toolkit for 1D ultrafast dynamics in condensed matter. *Comput. Phys. Commun.* **2014**, *185*, 651–660.

29. Nasiri, S.; Dashti, A.; Hosseinnezhad, M.; Rabiei, M.; Palevicius, A.; Doustmohammadi, A.; Janusas, G. Mechanochromic and thermally activated delayed fluorescence dyes obtained from D–A–D' type, consisted of xanthen and carbazole derivatives as an emitter layer in organic light emitting diodes. *Chem. Eng. J.* **2022**, *430*, 131877.

30. Schmising, C.V.K.; Bargheer, M.; Kiel, M.; Zhavoronkov, N.; Woerner, M.; Elsaesser, T.; Vrejoiu, I.; Hesse, D.; Alexe, M. Coupled ultrafast lattice and polarization dynamics in ferroelectric nanolayers. *Phys. Rev. Lett.* **2007**, *98*, 257601.

31. Schmising, C.V.K.; Harpoeth, A.; Zhavoronkov, N.; Ansari, Z.; Aku-Leh, C.; Woerner, M.; Elsaesser, T.; Bargheer, M.; Schmidbauer, M.; Vrejoiu, I.; et al. Ultrafast magnetostriction and phonon-mediated stress in a photoexcited ferromagnet. *Phys. Rev. B* **2008**, *78*, 060404.

32. Schick, D.; Herzog, M.; Bojahr, A.; Leitenberger, W.; Hertwig, A.; Shayduk, R.; Bargheer, M. Ultrafast lattice response of photoexcited thin films studied by X-ray diffraction. *Struct. Dyn.* **2014**, *1*, 064501.